Investigation of Directional Reflectance in Boreal Forests with an Improved Four-Scale Model and Airborne POLDER Data

Sylvain G. Leblanc, Patrice Bicheron, Jing M. Chen, Marc Leroy, and Josef Cihlar

***Abstract*— Airborne Polarization and Directional Earth Radiation (POLDER) data acquired during the boreal ecosystem-atmosphere study (BOREAS) and the four-scale model of Chen and Leblanc [10] are used to investigate radiative transfer in boreal forest. The four-scale model is based on forest canopy architecture at different scales. New aspects are incorporated into the model to improve the physical representation of each canopy, as follows:**

1) **Elaborate branch architecture is added.**
2) **Different crown shapes are used for conifer and deciduous forests.**
3) **Bilayer version of the model is introduced for forest canopies with an important understory.**
4) **Natural repulsion effect is considered in the tree distribution statistics.**

Ground measurements from BOREAS sites are used as input parameters by the model to simulate measurements of bidirectional reflectance distribution function (BRDF) from four forest canopies (old black spruce, old aspen, and old and young jack pine) acquired by the POLDER instrument from May–July 1994. The model is able to reproduce with great accuracy the BRDF of the four forests. The importance of the branch architecture and the self-shadowing of the foliage is emphasized.

***Index Terms*—BRDF, canopy architecture, POLDER, radiative transfer.**

NOMENCLATURE

b	Major axis of the spheroid crown shape.
B	Domain size.
D	Number of trees in the domain B.
F_O	Repulsion effect function.
$G(\theta)$	Projection of unit leaf area.
$G_b(\theta)$	Projection of unit branch silhouette area.
$G_L(\theta)$	Projection of unit branch leaf area.
H	Effective height $(H_a + H_b + \frac{1}{3} H_c)/\cos(\theta_s)$.
H_a	Height of the lower part of the tree (part with no foliage).
H_b	Height of the cylinders.
L	Leaf area index (LAI).
L_b	Branch silhouette area index.
L_H	LAI accumulated horizontally.
L_E	Effective LAI for one crown.
L_L	Branch LAI.
L_o	LAI accumulated.
m_2	Cluster mean size.
n	Number of quadrats in the domain B.
P_G	Probability of seeing illuminated ground area.
$P_{\text{gap}}(\theta)$	Gap probability within a tree at the angle θ.
P_{ig}	Probability of having an illuminated ground area.
P_{vg}	Probability of viewing the ground (gap fraction).
P_{ti}	Proportion of tree crown illuminated in the viewer direction.
P_T	Probability of viewing sunlit trees crowns.
P_{tj}	Overlapping of j trees.
r	Radius of the tree crowns.
R^2	Coefficient of determination.
$\overline{s}(\theta)$	Mean path length within a canopy.
R_G	Ground reflectivity.
R_b	Branch thickness-length ratio.
R_L	Leaf (or shoot) thickness-length ratio.
R_T	Foliage reflectivity.
R_{ZG}	Shaded ground surface reflectivity.
R_{ZT}	Shaded foliage reflectivity.
R	Total reflectance.
$S_g(\theta_v)$	Crown projection on the ground in the sun beam direction.
$V_g(\theta_v)$	Crown projection on the ground in the viewer direction.
W_s	Mean width of element shadow cast inside tree crowns.
α	Half apex angle.
α_b	Branch inclination from horizontal.
α_L	Leaves or shoots orientation from horizontal.
γ_E	Needle-to-shoot area ratio.
$\Gamma(\xi)$	Shadowing phase function of the foliage density.
μ	Foliage density (inside crown).
Ω_E	Clumping index of the crown element.
ξ	Angle difference between the sun and the viewer.
ϕ	Azimuth angle difference between the sun and the viewer.
θ_s	Solar zenith angle.
θ_v	View zenith angle.

Manuscript received March 19, 1997; revised September 10, 1998.

S. G. Leblanc, J. M. Chen, and J. Cihlar are with the Canada Center for Remote Sensing, Ottawa, Ont., Canada K1A 0Y7 (e-mail: sylvain.leblanc@ccrs.nrcan.gc.ca).

P. Bicheron and M. Leroy are with the Centre d'études spatiales de la biosphère (CESBIO), 31401 Toulouse Cedex, France.

Publisher Item Identifier S 0196-2892(99)03463-4.

I. INTRODUCTION

IT IS A well-known fact that the angular reflectance of the earth vegetation surface is anisotropic. The reflectance of forest canopies has been studied using satellite [12], [36] and ground-based measurements [14] or models [24]. Modeling the bidirectional reflectance distribution function (BRDF) is

necessary for the understanding of the information contained in remote-sensing measurements and a critical step in determining biological properties of canopies. Dense forests and crop fields have been simulated by turbid-media radiative transfer models [16], [26], [28], [33]. For sparse forests, geometric-optical models [19], [20], [27], [32] have been used. Validations of such BRDF models using remote-sensing measurements [21], [29] increases the understanding of physical processes in forest canopies. A rigorous validation of a model requires *in situ* measurements of biophysical parameters with simultaneous remote-sensing measurements.

During the Boreal Ecosystem-Atmosphere Study (BOREAS) project [30], conducted in Canada, airborne BRDF measurements were collected using the POLarization and Directional Earth Radiation (POLDER) instrument. The instrument consists of a CCD matrix with a very wide field of view and a rotating filter wheel [13]. It is well adapted to the characterization of the hotspot [2] and allows the derivation of directional measurements on each grid point of extended areas [17]. Several data sets of BRDF measurements were consequently acquired over different boreal conifer and deciduous forests during spring and summer 1994 in the southern study area of BOREAS [1]. The differences of angular signatures from deciduous and conifers forest must be investigated by taking into account the biophysical and structural parameters specific to each canopy type. The effects of forest canopy architecture on remote-sensing measurements have been closely studied in recent years [4], [8], [15]. One way to understand airborne measurements is to simulate the radiative transfer processes in the forest using a model that closely represents the physical reality.

The four-scale radiative transfer model [10] introduced several physical aspects that have not been adequately considered in previous models: the canopy consists of a nonrandom distribution of discrete trees with structural components, such as branches, shoots, and leaves or needles. The hotspot is modeled on both the canopy and the ground and calculated based on a canopy-gap size distribution. Tree crown surfaces are treated as a three-dimensional (3-D) medium in which mutual shadows of leaves (or shoots for conifers) can be observed even on the sunlit side of the crown.

In this paper, new aspects are added to the model. It is now possible to specify the branches and leaves' orientations within the tree crowns. The natural repulsion effect on the tree distribution is now simulated. A spheroid crown shape with its specific foliage self-shadowing is used to model deciduous species. Furthermore, canopy sites, which contain an important understory, can be simulated with a double-canopy version of the model.

Four canopy sites, old black spruce, old and young jack pine, and old aspen are investigated with emphasis on their structural differences by comparing the POLDER measurements with four-scale in two ways: the first consists of direct BRDF comparisons in the principal and perpendicular planes and the second uses the instrumental configuration to compose a BRDF with a high angular resolution. These comparisons also serve to demonstrate the four-scale model versatility. The importance of the branch architecture and the self-shadowing of the internal foliage in the crown is shown by comparing outputs of the model with and without these considerations.

II. Four-Scale Model

The four-scale model was developed by Chen and Leblanc [10] as an improvement over previous geometric-optical models. The model focuses on the mathematical description of forest canopy architecture at various scales.

Trees are modeled as discrete objects; for conifers, four-scale uses a cone plus a cylinder shape [27] (see Fig. 1) to represent the crown. The crown's surface is treated as a complex medium in which shoots (or leaves for deciduous canopies) can cast shadows on each other so that even on the sunlit side of a crown, the viewer can see shaded foliage. The patchiness of the stand tree distribution is simulated with the Neyman type A distribution [25]. The Neyman distribution uses the probability of having groups of trees randomly distributed in a forest. Both the group size and the location of the group follow a Poisson distribution; hence, the notation double Poisson distribution is also used to describe it. The gap fraction is computed using the Neyman distribution with an averaged gap probability within the tree crowns and a negative binomial function. These functions allow the sun's beam and view line penetration into multiple trees to compute the overlapping of the crowns. The hotspot is modeled with two kernels, one uses the gap size distribution within the crowns for the canopy hotspot and the other one uses the gap size distribution between the tree crowns for the ground hotspot. The size of the leaves or shoots, the density of tree stands, and the crowns size are important factors in determining the shape of the hotspot.

The model parameters can be separated in three categories, as follows:

1) sites parameters (domain size, LAI, tree density, tree grouping index with quadrant size, and solar zenith angle);
2) tree architecture parameters (crown radius and height, apex angle, needle-to-shoot ratio, foliage clumping index, and tree foliage typical size);
3) reflectivities of the foliage and the ground.

These later parameters depend on the sensor and the wavelength used and thus can be seen as more adjustable than the architectural parameters.

The model finally computes four surface proportions: foliage illuminated (P_T), foliage shaded (Z_T), and ground illuminated (P_G) and shaded (Z_G). Each proportion is multiplied by its reflectivity factor that depends on the wavelength used

$$R = P_T \cdot R_T + Z_T \cdot R_{ZT} + P_G \cdot R_G + Z_G \cdot R_{ZG}. \quad (1)$$

A. Branch Architecture

To improve the radiation transfer simulation within the crowns in the four-scale model, a substantial branch architecture is included in this paper. This architectural level is an important aspect of forest canopies because of the

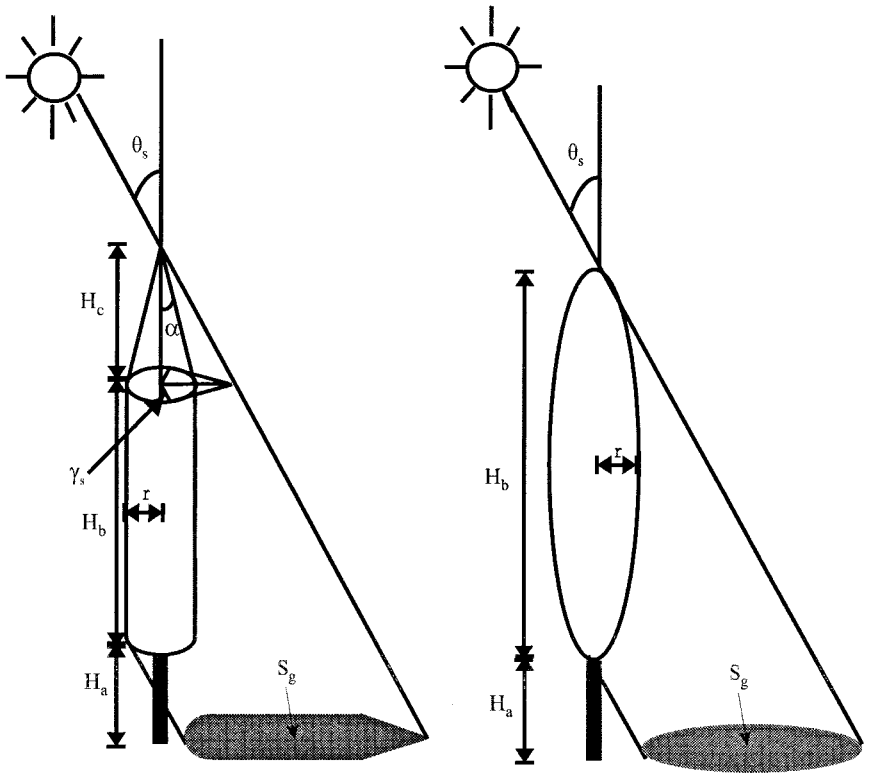

Fig. 1. Geometric shapes of the crown: (a) cone-cylinder for conifers and (b) spheroid for deciduous.

difference in branch and leaf spatial and angular distribution patterns among the different species. In conifer stands, shoots usually act as the foliage elements in radiation interception. Chen and Black [6] developed a mathematical description of branch architecture for radiative transfer models. Using the same basic formulation, with the addition of a more realistic branch structure with leave (or shoot for conifers) and branch thickness, the branch architecture is adapted for discrete trees. This enables the study of the effects of the branch and leaf orientations on the radiative transfer processes. The following assumptions are made.

1) Leaves (or shoots) are the foliage elements (scatterers).
2) Foliage clumping occurs at both the branch and needle levels; the branch level clumping is implicit in the branch architecture.
3) A branch is a flat slab of foliage whose thickness is small but not negligible compared with other dimensions.
4) Foliage element is a 3-D object whose thickness is small but not negligible compared with its other dimensions.
5) Elements are randomly distributed spatially within the confinement of the silhouette of each branch.
6) Normal to each branch at a fixed angle to the vertical is randomly oriented azimuthally around the center of the tree.
7) Branches are confined in discrete tree silhouettes.

In four-scale, the probability of a beam passing through an individual crown is expressed [10] as

$$P_{\text{gap}}(\theta) = e^{-G(\theta)L_o \cdot \Omega_E/\gamma_E} \tag{2}$$

where $G(\theta)$ is the projection of unit leaf area (θ can either be the zenith angle for the sun's beam θ_s or for the view line θ_v), Ω_E is the clumping index of the crown's scatterers, γ_E is the needle-to-shoot area ratio, which is unity for nonconiferous trees, and $L_o = \mu \cdot \overline{s}(\theta)$ is the LAI accumulated over the path of the sun's beam or view line that depends on the foliage density $\mu = L/(V \cdot D/B)$ and the mean path $\overline{s}(\theta) = V/S \cdot \cos(\theta)$ in one tree crown, where V is the volume of the crown, D is the number of stem per domain, B is the size of the domain, S is the projection of the tree crown on the ground, and, L is the LAI of the stand. Previously, with $G(\theta) = a - b\theta$, it has been possible to simulate some architecture within the crowns, but $G(\theta)$ can be found for a specific branch structure. We define an effective projection of unit leaf area as

$$G_E(\theta) = G(\theta) \cdot \Omega_E/\gamma_E \tag{3}$$

so (2) becomes

$$P_{\text{gap}}(\theta) = e^{-G_E(\theta)L_o}. \tag{4}$$

The branch architecture will serve to compute $G_E(\theta)$ directly from the orientations of the branches and leaves. Fig. 2 is a schematic representation of a branch architecture for a conifer. In this representation, a branch can be seen as a "large porous leaf."

The probability of j branch overlapping in the direction of the beam over a length $\overline{s}(\theta)$ can be expressed using the

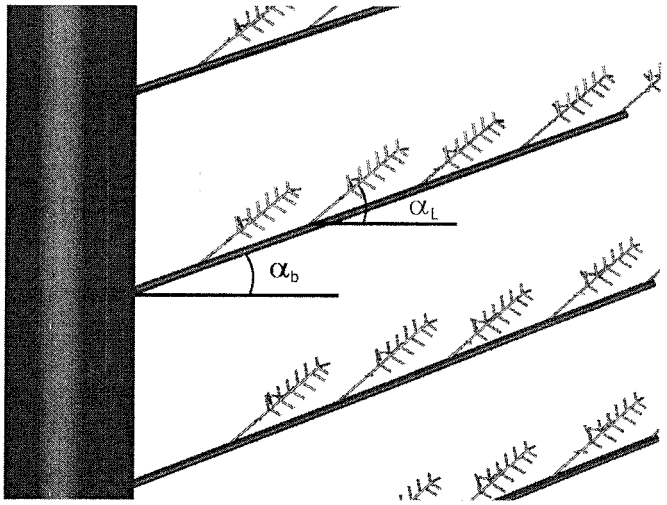

Fig. 2. Schematic representation of the branch architecture for a conifer.

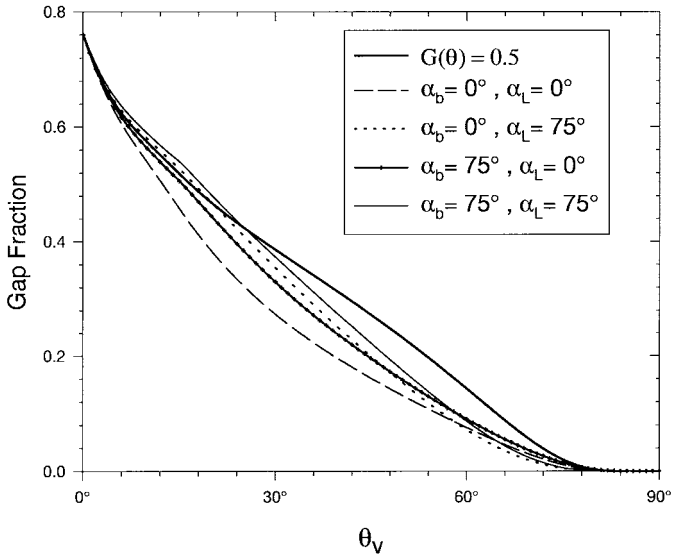

Fig. 3. Effect of the branches architecture on the gap fraction.

Poisson distribution as [6]

$$P_{bj}(\theta) = [G_b(\theta)L_{ob}]^j \cdot \frac{e^{-G_b(\theta)L_{ob}}}{j!} \tag{5}$$

where

$$L_{ob} = \mu_b \cdot \overline{s}(\theta) \tag{6}$$

is the branch silhouette area index accumulated over the path within the crown and

$$\mu_b = L_b/(V \cdot D/B) \tag{7}$$

is the branch silhouette density, L_b is the branch silhouette area index, defined as the total branch silhouette area per unit of ground surface area. L_b is related to the LAI as

$$L = L_b L_L \tag{8}$$

where L_L is the branch LAI defined as one-half of the total leaf area within a branch divided by the branch silhouette area. $G_b(\theta)$ is the mean projection of unit branch silhouette area in the direction of the beam and is first calculated with

$$G_b'(\theta) = \begin{cases} \cos\alpha_b \cos\theta, & \theta \le \pi/2 - \alpha_b, \\ \cos\alpha_b \cos\theta\left[1 + \dfrac{2(\tan x - x)}{\pi}\right], & \theta > \pi/2 - \alpha_b \end{cases} \tag{9}$$

and

$$x = \cos^{-1}(\cot\alpha_b \cot\theta) \tag{10}$$

where α_b is the branch inclination from the horizontal. $G_b'(\theta)$ is valid for flat branches with negligible thickness. For branches with thickness, it becomes

$$G_b(\theta) = G_b'(\theta) + \sin\left[\cos^{-1}(G_b'(\theta))\right] R_b \tag{11}$$

where R_b is the ratio of the thickness of a branch (arbitrarily taken in this paper as 0.1 m) over its length ($r/\cos\alpha_b$). The probability of a beam travelling through gaps between leaves within a branch oriented at an angle β with respect to the beam azimuthal direction is determined by the branch LAI (L_L), and the incident angle (θ_b) of the beam to the normal to the branch. θ_b is defined as

$$\cos\theta_b = |\sin\theta \sin\alpha_b \cos\beta + \cos\theta \cos\alpha_b|. \tag{12}$$

Branches are symmetrically distributed around the center of the trees; hence, the probability of a beam passing through one branch is

$$P_{L1}(\theta) = \frac{1}{\pi}\int_0^{\pi} P_{L1}(\theta, \beta)\, d\beta \tag{13}$$

where

$$P_{L1}(\theta, \beta) = \exp\left[-G_L(\theta)L_L/\gamma_E \cos(\theta_b)\right]. \tag{14}$$

$G_L(\theta)$ is computed by replacing α_b by α_L in (9) and (11) and using the ratio R_L instead of R_b. R_L is the ratio of the thickness of a leaf over its length. This ratio is larger for conifers than deciduous trees because it expresses the thickness of the shoot over its length. α_L is the leaf inclination from the horizontal. The probability of a beam passing through j branches without interception is found by multiplying the probability of passing through one branch j times

$$P_{Lj}(\theta) = \prod_{i=0}^{j} P_{L1}(\theta) = P_{L1}^j(\theta). \tag{15}$$

The probability of a beam encountering and passing through j layers of branches without interception is then found by multiplying the probability of having j overlappings of the branches by the probability of passing through j branches

$$P_j(\theta) = P_{bj}(\theta)P_{Lj}(\theta). \tag{16}$$

The summation of all probabilities of $P_j(\theta)$ gives the probability that a beam passes through the tree crown

$$P_{\text{gap}}(\theta) = \sum_{j=0}^{n_b} P_j(\theta) \tag{17}$$

where n_b is the maximum number of branches that can be encountered along the mean path $\overline{s}(\theta)$. From this, we can

TABLE I
MODEL INPUT PARAMETERS FOR THE FOUR CANOPIES OLD BLACK SPRUCE (OBS), YOUNG JACK PINE (YJP), OLD JACK PINE (OJP), AND OLD ASPEN (OA)

		OBS	YJP	OJP	OA aspen/hazelnut (single)
Site Parameters	Latitude N	53.985°	53.975°	53.916°	53.629°
	Longitude W	-105.12°	-104.65 °	-104.69°	-106.20°
	Domain size	1 ha	1 ha	1 ha	1 ha
	θ_s	33.5°	37.2°	35.0°	39.3°
	LAI	4.5	2.7	2.2	1.5 / 0.5 (1.5)
	Tree Density	4000 trees/ha	4000 trees/ha	1850 trees/ha	850 / 6000 trees (850) /ha
	Tree grouping (m_2)	4	3	3	3 / 0
	Quadrat size	500 m^2	500 m^2	500 m^2	285.7 m^2
Tree Architecture Parameters	H_a	0.5 m	0.5 m	7.0 m	11.0 / 0.0 (11.0) m
	H_b	6.5 m	2.5 m	4.0 m	7.0 / 2.0 (7.0) m
	$H_c(\alpha, r)$	1.9 m	1.5 m	3.2 m	–
	r	0.45 m	0.85 m	1.30 m	1.90 / 1.00 (1.9) m
	α	13°	30°	22°	–
	α_b	–	15°	15°	–
	α_L	–	80°	80°	–
	L_L	–	0.8	0.8	–
	$G(\theta)$	0.5	–	–	0.5 / 0.5 (0.5)
	W_s	0.035 m	0.17 m	0.05 m	0.10 / 0.02 m (0.10)
	γ_E	1.41	1.43	1.30	–
	Ω_E	0.70	–	–	0.80/0.98 (0.8)
	R_L	–	0.2	0.2	–
	R_b	–	0.1 m	0.1 m	–
Reflectivities	R_T (red)	0.11	0.05	0.07	0.07 / 0.06 (0.07)
	R_{ZT}(red)	0.003	0.005	0.003	0.01 / 0.02 (0.01)
	R_T (nir)	0.50	0.53	0.53	0.50 / 0.50 (0.5)
	R_{ZT}(nir)	0.11	0.19	0.13	0.20 / 0.30 (0.20)
	R_G (red)	0.04	0.05	0.09	0.04 (0.05)
	R_{ZG}(red)	0.002	0.004	0.003	0.02 (0.01)
	R_G (nir)	0.25	0.15	0.17	0.20 (0.25)
	R_{ZG}(nir)	0.11	0.08	0.09	0.15 (0.2)

compute the effective projection of unit foliage $G_E(\theta)$ by equating (4) and (17)

$$G_E(\theta) = \frac{\ln\left[1 \Big/ \sum_{j=0}^{n_b} P_j(\theta)\right]}{L_o}. \tag{18}$$

Both (17) and (18) are then used in the model instead of (3) and (4). Fig. 3 shows the effect of the branch architecture on the gap fraction for a black spruce stand, the parameters used are the same as for the POLDER comparison found in Table I. The effects of the branch architecture on the gap fraction vary greatly with the view angle because the overlapping crown probability has an important role in the gap fraction computation. The case in which both the branches and shoots are horizontal ($\alpha_b = 0°$ and $\alpha_L = 0°$) gives the lowest gap fraction for most view zenith angles (θ_v). The penetration within one crown increase as the view angle approaches 75°, but the view line penetrates so many crowns that the resulting gap fraction is similar to the other simulated branch structures. Only the random case [simulated with $G(\theta) = 0.5$] gives a larger gap fraction for view zenith angles larger than 60°. At nadir, the values are all very similar because of the large pathlength through the tree crowns. The main component of the gap fraction comes from gap in the canopy between the crowns, which is around 0.75 at nadir. When comparing the branches at 75° with horizontal shoots to the case in which the shoots are at 75° with horizontal branches, we see that larger gap fractions can be found in view zenith angle from 0° to around 50° for the more vertical shoots. When both the branches and the shoots are at 75°, the branch architecture increases the probability of seeing the ground near nadir and decreases it at larger view zenith angles.

In these branch architecture simulations, the length of the branches must not exceed the height of the crown as α_b gets close to 90°. For large values of α_b, it is preferable to use a fix value for R_b.

B. Spheroid Crown Shape

For the simulation of coniferous forests, the cone and cylinder crown shapes are suitable [10], [27]. For deciduous forest canopies, a spheroid shape like the one used by Li and Strahler [18] is more appropriate (see Fig. 1). The crown shape serves to determine the projected area on the ground and the volume of the crown that is used for the calculation of the mean path through a crown. The projected area of an individual crown on the ground in the viewer's direction (V_g) becomes

$$V_g = \frac{\pi r^2}{\cos(\theta'_v)} \tag{19}$$

where

$$\theta'_v = \tan^{-1}\left[\frac{b}{r}\tan(\theta_v)\right] \tag{20}$$

and $b = H_b/2$. Considering this new shape, the different terms in the probability of seeing illuminated foliage P_{Tf} [10], without taking into consideration the hotspot, are consequently modified. We have

$$P_{Tf} = P_{ti} \cdot Q_{1\text{tot}} + [1 - P_{ti}] \cdot Q_{2\text{tot}}. \tag{21}$$

Where P_{ti} is the observed proportion of illuminated surface for a spheroid shape, it is computed as [32]

$$P_{ti} = 0.5[1 + \cos\theta'] \tag{22}$$

where

$$\cos\theta' = \cos\theta'_s \cos\theta'_v + \sin\theta'_s \sin\theta'_v \cos\phi \tag{23}$$

and θ'_s is defined like θ'_v as

$$\theta'_s = \tan^{-1}\left[\frac{b}{r}\tan(\theta_s)\right]. \tag{24}$$

$Q_{1\text{tot}}$ represents the portion of observed sunlit imaginary surface occupied by sunlit foliage, and $Q_{2\text{tot}}$ is the proportion of viewed sunlit foliage on a self-shaded part of the crown. $Q_{1\text{tot}}$ and $Q_{2\text{tot}}$ are first computed over a single tree crown and then summed over all the trees reached over the view path (see Chen and Leblanc [10]). On a discrete crown, $Q_{1\text{tot}}$ and $Q_{2\text{tot}}$ are:

$$Q_1 = \Gamma(\xi)\left[1 - e^{-L_H(C_s+C_v)}\right]\left[\frac{C_s C_v}{C_s + C_v}\right] \tag{25}$$

and

$$Q_2 = \Gamma(\xi)\left[e^{-L_H C_s} - e^{-L_H C_v}\right]\left[\frac{C_s C_v}{C_v - C_s}\right] \tag{26}$$

where $\Gamma(\xi)$ is the geometric shadow function of the foliage elements as a function of ξ, which is found from $\cos\xi = \cos\theta_s\cos\theta_v + \sin\theta_s\sin\theta_v\cos\phi$ and L_H is the LAI accumulated horizontally in one tree crown. For conifers, $C_v = G_E(\theta_v)/\sin(\theta_v + \alpha)$ and $C_s = G_E(\theta_s)/\sin(\theta_s + \alpha)$, where α is the half apex angle of the cone. For the spheroid, C_v and C_s can be expressed as

$$C_s = \frac{\overline{s}(\theta_s) \cdot G_E(\theta_s)}{2 \cdot r} \tag{27}$$

$$C_v = \frac{\overline{s}(\theta_v) \cdot G_E(\theta_v)}{2 \cdot r}. \tag{28}$$

The mutual shadowing from one crown to another used in the four-scale model for simulating the proportion of sunlit crown with height was approximated by dividing the crown into two components: the cone and the cylinder and with the penetration through multiple crowns with $Q_{1\text{tot}}$ and $Q_{2\text{tot}}$. For the spheroid shape, the mutual shadowing effect is only considered with $Q_{1\text{tot}}$ and $Q_{2\text{tot}}$ with a minimal effect on the final proportions since the division of the crown into two components (sunlit and shaded) for the conifers serves only as a weighting factor for $Q_{1\text{tot}}$ and $Q_{2\text{tot}}$.

C. Overlapping of Tree Crowns with the Repulsion Effect

The overlapping of tree crowns computed by the four-scale model using the combined negative binomial and Neyman functions is often overestimated near the vertical view direction. The overestimation of the overlapping directly affects the calculation of the gap fraction. Allowing crowns to overlap at nadir, increases the gap fraction. In reality, tree overlapping in the vertical direction is very small due to the natural repulsion effect between trees in the competition for light. The overestimation of the overlapping computed is especially important for forest with large crown radius. If there is no overlapping of the crowns at nadir, the probability of seeing the ground (the gap fraction) is

$$P_{\text{vgn}}(\theta_v) = 1 - V_g(\theta_v) \cdot [1 - P_{\text{gap}}(\theta_v)] \cdot D/B \tag{29}$$

where $V_g(\theta_v)$ is the projection of one tree crown on the ground. $P_{\text{gap}}(\theta_v)$ is the gap probability within one tree and D/B is the tree density. In forest stands, trees can be found in clusters; therefore, as the view angle differs from nadir, there is a probability of overlapping. We assume that the gap fraction value (now denoted P_{vgo}) found with the negative binomial and the Neyman distribution is valid at large zenith angles. The resulting gap fraction is given by

$$P_{vg}(\theta_v) = P_{\text{vgo}}(\theta_v) + [P_{\text{vgn}}(\theta_v) - P_{\text{vgo}}(\theta_v)]\, F_O(\theta_v) \tag{30}$$

where $F_O(\theta_v)$ controls the rate at which the repulsion effect is reduced as the zenith angle increases. It is defined here as

$$F_O(\theta_v) = \exp\left[-\frac{(V_G(\theta_v) - V_G(\theta_v = 0)) \cdot P_{\text{vgo}}(\theta_v)}{V_G(\theta_v = 0) \cdot P_{\text{vgo}}(0)}\right]. \tag{31}$$

Fig. 4 shows the gap fraction with and without the repulsion effect. The effect is more pronounced for the jack pine simulation than for the black spruce one. Both forests have a density of 4000 stems per hectare, but the foliage density inside the crown is more dense for the black spruce forest. Because of the opacity of black spruce crowns, the chances of passing through more than one crown was diminished, so the overlapping did not change much of the gap fraction in the vertical direction, but the jack pine forest allows more penetration, so more overlapping means larger gap fractions. In the simulation, F_O can be multiplied by a factor 0 to 1, which represents the percentage of repulsion desired.

D. Bilayer Forest

Modeling forest canopies is often confronted by the complexities of mixed forests with trees of different shapes and sizes. Some special cases can be modeled with a few modifications of the four-scale model. The BOREAS old aspen site, which is composed of tall aspen trees and short hazelnut shrubs, presents a new challenge for BRDF modeling. To study this double-canopy structure (see Fig. 5), a new module is added to the four-scale model. For one-canopy structure, the BRDF is computed using (1) by attributing reflective factors to four surface proportions. When considering a second canopy, two new components are calculated: the second (lower) canopy illuminated and shaded components.

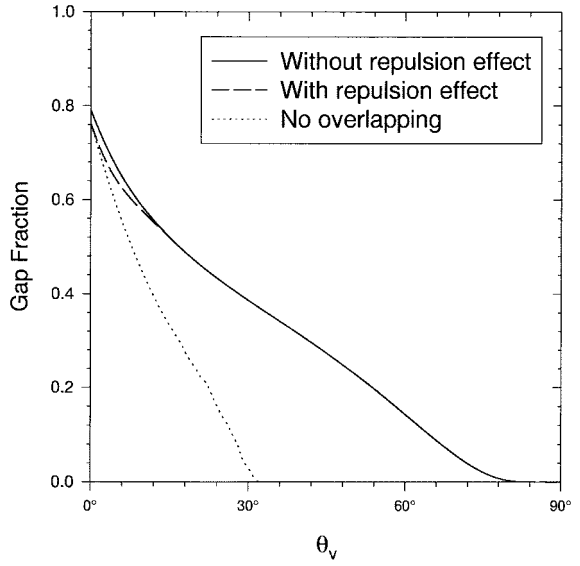

Fig. 4. Effects of the mutual repulsion effect in tree distribution on the gap fraction for (a) old black spruce and (b) young jack pine.

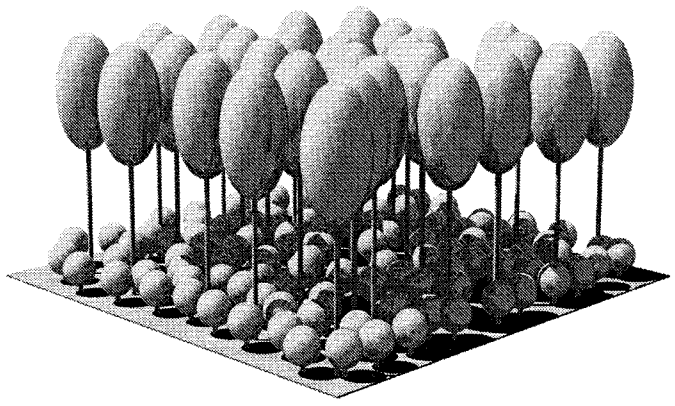

Fig. 5. Double-canopy representation for an old aspen forest with hazelnut understory.

Assuming that the lower canopy is much shorter than the upper one, the upper canopy is then independent of the lower one, i.e., the shadow cast by the lower canopy doesn't affect the view and illumination of the upper canopy. The new process can be separated in the following three steps.

Step 1: Original four-scale model is run with the parameters from the upper canopy, a subscript *1* is added to the notation for the upper canopy and subscript *2* for the lower canopy. The only parameter change is the effective height, which is used in the calculation of the ground hotspot kernel, that must be reduced to take into account the lower canopy. This is done by reducing the value of H_{a1} (the height of the part without foliage of the upper canopy) by the total height of the lower canopy ($H_{a2}+H_{b2}+H_{c2}$). The change in H_{a1} affects only the inbetween crowns hotspot calculation. Because the trees are assumed to be at equal height, the overshadowing of tree crowns does not depend on the crown base height.

Step 2: Original four-scale model is run with the parameters of the lower canopy. It must be noted that, for the hazelnut canopy, the overlapping of the crowns is allowed at nadir to better represents the real canopy.

Step 3: With the four components of Steps 1 and 2, plus the gap fraction from both canopies, the six portions of the double-canopy structure can be computed.

The two components of the upper canopy (P_{T1} and Z_{T1}) are taken directly from Step 1. The probability of seeing illuminated foliage on the lower canopy if the upper canopy is absent was computed in Step 2 (P_{T2}), but the solar beam that reaches the lower canopy and is reflected to the viewer has the probability of P_{G1}; thus, the probability of seeing illuminated foliage in the lower canopy in the presence of an upper canopy is simply

$$P_{T2'} = P_{G1} \cdot P_{T2}. \tag{32}$$

The probability of seeing shaded foliage in the lower canopy is found by subtracting the probability of seeing the illuminated lower canopy ($P_{T2'}$) from the probability of seeing the foliage in the lower canopy through the upper one ($P_{st2'}$)

$$Z_{T2'} = P_{st2'} - P_{T2'} \tag{33}$$

where

$$P_{st2'} = (1 - P_{vg2}) \cdot P_{vg1} \tag{34}$$

where P_{vg1} and P_{vg2} are the probabilities of seeing the background through the upper and lower canopy, respectively. The probability of seeing the ground illuminated under the bilayer canopy can be found by multiplying the probability of seeing the lower illuminated surface (ground or lower canopy) of both canopies

$$P_G = P_{G1} \cdot P_{G2}. \tag{35}$$

The sum of the six components must be unity; therefore, the probability of seeing the ground shaded can be found by subtracting the five probabilities from one

$$Z_G = 1 - P_{T1} - Z_{T1} - P_{T2'} - Z_{T2'} - P_G. \tag{36}$$

The total reflectance becomes

$$R = P_{T1} \cdot R_{T1} + Z_{T1} \cdot R_{ZT1} + P_{T2} \cdot R_{T2} + Z_{T2} \cdot R_{ZT2} + P_G \cdot R_G + Z_G \cdot R_{ZG}. \quad (37)$$

III. Comparison Between Model and Airborne POLDER Data

The improvements of the four-scale model described above, and the knowledge of ground biophysical parameters, permit the comparison of the measurements by the POLDER instrument and the model results.

A. Sites Description

The four boreal forests investigated in this paper were all BOREAS sites. Many optical and canopy architectural measurements were made during the experiment at the same sites by different teams. Those measurements are the basis for the four-scale model input parameters. They are summarized in the Table I.

1) Old Black Spruce: The old black spruce in the southern study area (SSA) is situated near Candle Lake, Sask., Canada. Typical black spruces (*Picea mariana*) have a crown shape consisting of a cone on top of a cylinder. The conical part generally has a denser foliage than the cylindrical part. The length of the cylinder is usually much greater than the height of the cone, and the foliage is close to the trunk. Below the crown is the trunk space, which has very little foliage. Black spruce trees have a horizontal branch structure with shoots mostly orientated parallel to the plane of the branches. The branches, around half a meter in length, are small compared to the height (5–10 m for the dominant trees) of the tree. Therefore, black spruce crowns have a pencil-like shape. Measurements show that, even with a horizontal branch architecture, the projection coefficient $G(\theta)$ is well approximated by a fixed value of 0.5 [4]. An LAI from four to six [11], with a clumping index Ω_E of 0.70 and a needle-to-shoots ratio γ_E of 1.41, were measured [9] for this site. Black spruce needles reflectivity ranges from 6 to 13% in the red band and around 40 to 50% in the near-infrared band. The old black spruce site has a density of around 4000 stems per hectare, with trees aged to 155 years. A crown closure of 0.42 was measured; therefore, the understory and the ground components are very important, especially near the vertical view direction. The understory is composed of smaller black spruce (1–5%) and Labrador tea, and the ground surface is covered by sphagnum moss. The ground surface has reflectivities lower than the foliage in both red (4–6%) and near-infrared band (around 25%). This site is not uniform, mainly because of the height variability and tree distribution.

2) Young Jack Pine: The young jack pine in SSA is also situated near Candle Lake. The form of the tree crown is not as well defined as it is for the black spruce. A cone and cylinder-like shape can still be seen in many trees, but it is more irregular and the cylinder is less elongated than the black spruce. A density of 4000 stems per hectare was measured on this site. The young jack pine crown radius is larger than the old black spruce trees at around 1 m with a mean tree height between 4 and 5 m. Jack pines (*pinus banksiana*) have near-horizontal branches, but the subbranches and shoots are more vertical. The main axes of the shoot are mostly between 5 and 10°, with a maximum between 10 and 30° from the zenith [4]. With an LAI of 2.6–3.1 [11], the crown foliage density is lower for the young jack pine than for the black spruce, which gives a crown closure similar to the black spruce site (0.43). The needle-to-shoot ratio γ_E was found to be 1.43 [9]. The needle reflectivity for jack pine trees is lower than the black spruce in the red with 5 to 8% but a little higher in the near-infrared with 50 to 55%. The average age of the young jack pine tree is between 11 and 16 years old. Jack pine forests are often found on sites after fires and almost even age. This site does not have an important understory, but the ground cover is composed of grasses, bearberry, and some lichens.

3) Old Jack Pine: The southern old jack pine site is situated near the young jack pine site. This forest has a lower tree density than the young jack pine site, with 1850 stems per hectare and an LAI of 2.0–2.5 [11]. This yields a crown closure of only 0.31. The trees are 12–15 m in height. The old jack pines exhibit large crowns with a mean radius between 1.25 and 1.5 m. From visual observations, a branch architecture similar to young jack pines is found in older jack pine. The needle-to-shoot ratio is smaller in the old jack pine than the younger ones, with γ_E = 1.28. The trees are around 60–75 years old. Opposite to the old black spruce stand, which has many small young black spruce as its understory, the old jack pine background is very reflective and mainly composed of lichens that appear in white colors.

4) Old Aspen: The old aspen site is located in the Prince Albert National Park, Sask., Aspen (*Populus tremuloides*) are the major deciduous species in the boreal environment and cover approximately 20% of the southern boreal landscape. The aspen site has trees at an even age of about 70 years. The density of the old aspen site is the lowest of the four canopies investigated in this paper, with around 850 stems per hectare [7]. The aspens are very tall, with an average height of 21.5 m. Most of the leaves and branches are found in the upper 7-m part of the canopy, which has a large trunk space. The foliage area varies considerably during the year. A maximum LAI of 2.4 was found around mid-July 1994. An important understory composed of hazelnut (*Corlus cornuta*) is present with a maximum LAI of more than three from around mid-June to the end of August. The monthly variation in LAI is very sharp during the month of May. LAI increases from zero to around two while buds emerge in late April followed by leaf emergence beginning in mid-May. The senescence of both overstory and understory begin in the middle of September. The aspen canopy has a clumping index Ω_E varying from 0.7 to 0.85, but the hazelnut is mostly unclumped (Ω_E = 0.98). The leaf reflectivity of the aspen canopy is around 5 to 10% in the red and 40 to 50% in the near-infrared.

B. POLDER Data

1) The POLDER Instrument: The airborne POLDER instrument is a radiometer designed to measure the directionality and polarization of the solar radiation scattered by

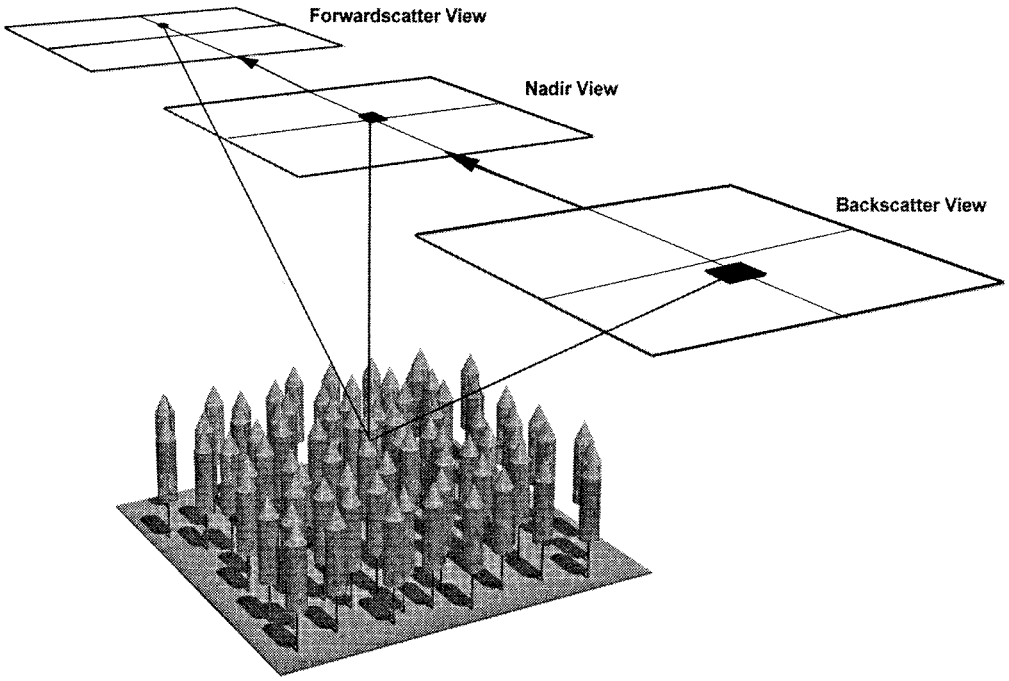

Fig. 6. POLDER data acquisition principle. The drawing shows three different positions of the aircraft representing three view angles for the same area.

the earth surface–atmosphere system [13]. The instrument produces bidimensional pictures of the ground on a CCD matrix (288 lines $\times$ 384 columns), allowing the observation of a given pixel in consecutive images under various viewing angles, as shown in Fig. 6. The zenith angular coverage is $\pm 51^\circ$ in the along-track direction and $\pm 43^\circ$ in the cross-track direction. Through a rotating filter wheel carrying spectral filters and polarizers by steps of 60°, measurements are acquired in five spectral bands: 443 nm (three directions of polarization), 550 nm, 670 nm, 864 nm (three directions of polarization), and 910 nm. The bandwidth range is from 10 to 20 nm, depending on the band. The ground pixel size is proportional to the instrument altitude. It is 35×35 m^2 for an altitude of 5500 m, which was generally flown by the aircraft C-130 during the BOREAS experiment. A sequence of ten acquisitions, corresponding to ten positions on the filter wheel, is performed within 3 s. The sequences are repeated every 10 s.

Several calibrations of the POLDER instrument were made before and after the BOREAS experiment on May 11 and October 24, 1994, respectively, at Laboratoire d'Optique Atmophérique, Lille, France, and during the campaign on May 27 and July 21, 1994, using a 30-in diameter portable hemisphere [22] operated by NASA Goddard Space Flight Center, Greenbelt, MD. The derived values of the absolute calibration coefficients are alike, with an average-peak discrepancy generally on the order of 5%, depending on the band [1]. It allows the conversion of POLDER measurements into radiances, then into reflectances, after taking into account the exoatmospheric solar irradiance and the zenith angle.

2) Data Acquisition: Mounted onboard the C-130 airplane from NASA-Ames, the POLDER instrument acquired multiple images in the principal, perpendicular, and oblique planes relative to the sun over the sites of the BOREAS SSA during the first two Intensive Field Campaigns (IFC-1 and IFC-2) from May to July 1994. POLDER recorded the aircraft position and altitude and gave the approximate position of a given pixel in any image. Ground control point techniques are used to fine-tune the geometric coregistration of the whole set of images of each flight. For each POLDER image, the pixel value of the CCD matrix yields a single directional spectral reflectance. Therefore, the processing of successive images permits the reconstruction of the BRDF for each tower site, averaged for a 175×175 m^2 area. For a typical C-130 flight altitude and speed, an angular step of approximately 10° is obtained, as shown in Fig. 7(d) and (c) for the sites old aspen (May 26), and old jack pine (July 21), respectively.

The POLDER concept also allows the derivation of directional measurements on each grid point of extended areas surrounding the tower site. This has been applied to the data sets of old black spruce and young jack pine, acquired on July 21, for an area of 5×5 km^2, with a spatial resolution degraded to 100×100 m^2. For a sharp investigation of forest directional reflectance, the "typical" BRDF of POLDER, as shown in Fig. 7(c) and (d), does not use the optimal angular resolution that can be achieved by POLDER. For both data sets of old black spruce and young jack pine, we suppose that the adjacent pixels of the supersites are identical to those of the supersites within an area of 900×900 m^2. This hypothesis is judged realistic because it is known from available cover maps that all pixels within the window of 81 pixels belong to the same species. All of these pixels have a directional sampling slightly different from each other because they are observed under different angular conditions. Therefore, collecting BRDF measurements on points within 900 m from the tower sites and superimposing them, we compose a new BRDF with a high directional resolution. As about 40 reflectance measurements

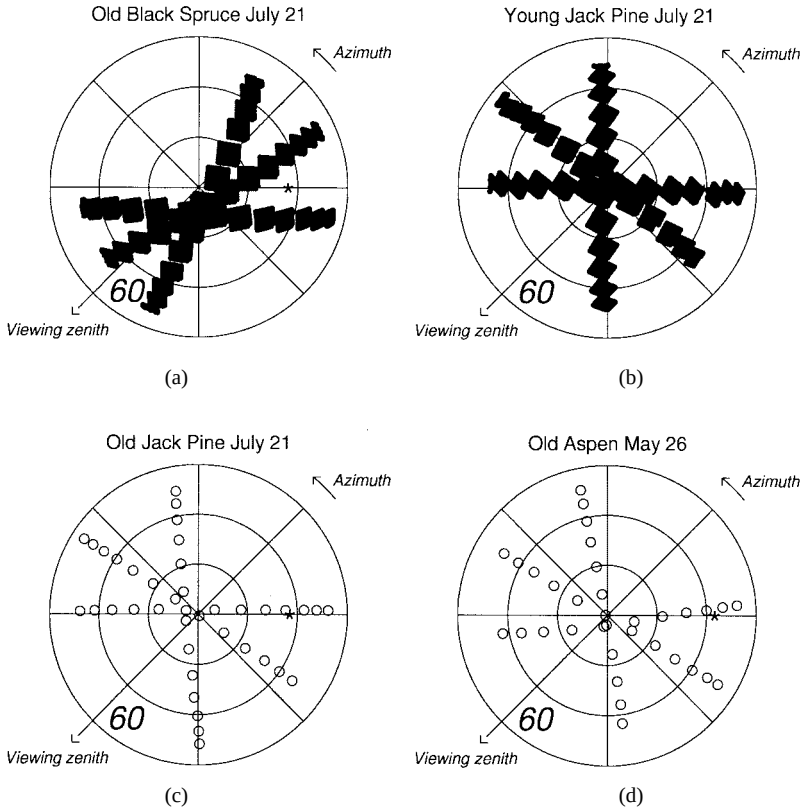

Fig. 7. Angular distribution of the measurements. The asterisks mark the positions of the sun (hotspot). (a) Old black spruce, (b) young jack pine, (c) old jack pine, and (d) old aspen.

per pixel are obtained, a complete BRDF with 3240 points (81 pixels $\times$ 40 reflectance) is thus produced from both sites [Fig. 7(a) and (b)]. Although the 81 pixels in each site seem to have quite a large tree height variation (7.5–12.5 m for old black spruce, 2.5–7.5 m for young jack pine), the dominant trees are more similar. The height variation, not included in the model, can underestimate the amount of shaded foliage in the smaller trees due to the shadow cast by taller trees.

The atmospheric correction algorithm 6S [34] is applied to each measurement. The aerosol optical depth of the full atmosphere and the fraction below the aircraft, obtained from the BORIS database, were interpolated at 550 nm and used as inputs to the algorithm. The following values were, respectively, deduced for the total and below-aircraft optical depths: old aspen (0.115, 0.075), young jack pine (0.115, 0.090), old jack pine (0.120, 0.095), and old black spruce (0.135, 0.070). Moreover, a mid-Arctic summer atmospheric model and a continental aerosol model were selected to characterize the atmosphere above the BOREAS sites. These assumptions may induce slight errors in the procedure, which are not expected, however, to deeply modify the magnitude and shape of the resulting BRDF.

C. Results

Table I shows the parameters used as input to the four-scale model for each site taken from ground-based measurements made during BOREAS. The reflectivity factors of the four components that composed the BRDF are based on ground measurements [3], [23], [31], [35].

The plots of either the principal or the perpendicular plane shown in this section were modeled discretely at the same view and solar angles as the measurements. This method of representation was chosen since the aircraft was not flying exactly in the perpendicular or principal solar plane. Continuous BRDF simulations can be seen in Figs. 14 and 15.

For the comparison between the model and the measurements, the regression factor (coefficient of determination) R^2 and the rms difference are used as quantificative guides. R^2 is generally an indication of the curves similarity, and the rms indicates the numerical accuracy. Table II has the R^2 and rms values for all simulations. The convention used here is that the backscattering side is plotted with negative view zenith angles. For the perpendicular plane, the half plane that was closer to the backscattering side has been assigned to the negative θ_v.

1) Old Black Spruce: Fig. 8(a) and (b) show the comparison between the model and POLDER data in the red band. R^2 of 0.97–0.95 and rms of 0.0042–0.0043 are found for the principal and perpendicular sites, respectively. Overall, the model slightly overestimates the measurements. Note that, from Fig. 7(a), the case presented in Fig. 8(a) was about 10° from the principal solar plane, so the peak at the hotspot was not reached. The near-infrared modeling shows a very good agreement between the model and the measurements with R^2 of 0.99 and 0.98 and rms of 0.0122 and 0.0058 for the principal and the perpendicular planes, respectively. The only difference on the principal plane [Fig. 8(c)] can be seen on the backscattering side, for view angles greater than the sun angle, where the model shows lower reflectance values than

TABLE II
COEFFICIENT OF DETERMINATION R^2 AND RMS DIFFERENCES BETWEEN FOUR-SCALE AND THE FOUR TOWER SITES

R2	OBS			YJP			OJP		OA double/single	
	Principal	Perpendicular	Spatialized	Principal	Perpendicular	Spatialized	Principal	Perpendicular	Principal	Perpendicular
RED	0.97	0.95	0.97	0.97	0.85	0.57	0.99	0.99	0.93/0.94	0.82/0.82
NIR	0.99	0.98	0.99	0.98	0.00	0.92	0.97	0.26	0.89/0.88	0.37/0.31

RMS	OBS			YJP			OJP		OA double/single	
	Principal	Perpendicular	Spatialized	Principal	Perpendicular	Spatialized	Principal	Perpendicular	Principal	Perpendicular
RED	0.0042	0.0043	0.0022	0.0020	0.0038	0.0094	0.0011	0.0013	0.0027/0.0029	0.0013/0.0039
NIR	0.0122	0.0058	0.0058	0.0092	0.0100	0.0012	0.0366	0.0246	0.0224/0.0196	0.0225/0.0142

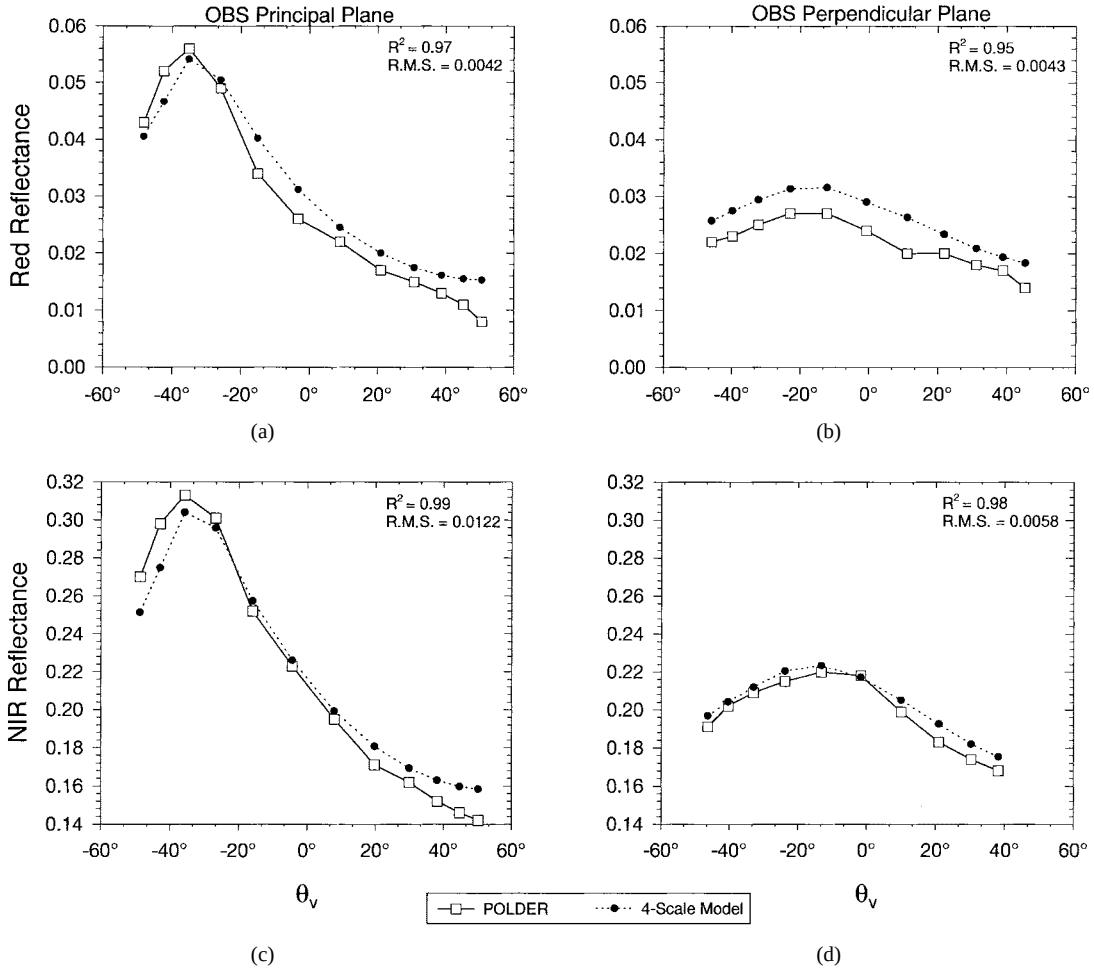

Fig. 8. Comparison between POLDER and four-scale for the old black spruce site: (a) principal plane red band, (b) perpendicular plane red band, (c) principal plane near-infrared band, and (d) perpendicular plane near-infrared band.

POLDER. This effect was also seen in a previous study [10], in which the model was compared to PARABOLA data at view zenith angles larger than 60°. This small discrepancy may be explained by a systematic error in the self-shadowing scheme ($Q_{1\mathrm{tot}}$) that seems to underestimate the amount of sunlit foliage and the angle independant multiple scattering used to compute the shaded reflectivities. The perpendicular planes [Fig. 8(b) and (d)] are well reproduced by the four-scale model, with very good rms and R^2 values for both planes. Other comparisons between the model and measurements made with data sets from other dates, with different solar angles, give similar agreements between the model and the measurements.

Using the parameters of the tower site, the spatialized data set is compared with the model in Fig. 9. Each grid point (every 5°) in Fig. 9(a) and (b) is a weighted interpolation of the measurements. The interpolation averages the measurements and removes some effects of the inhomogeneity of the forests. Each grid point corresponding to a specific θ_v (0–60°) and ϕ (0–360°) is then simulated using an averaged θ_s of 33.5° to give Fig. 9(c) and (d). For both bands, the model and the measurements have the same general shape except in the hotspot region. The aircraft flight did not allow measurements to be taken close enough to the principal plane so that the maximum in reflectance was not reached. There is a double peak in the measurements because, in theory, it is

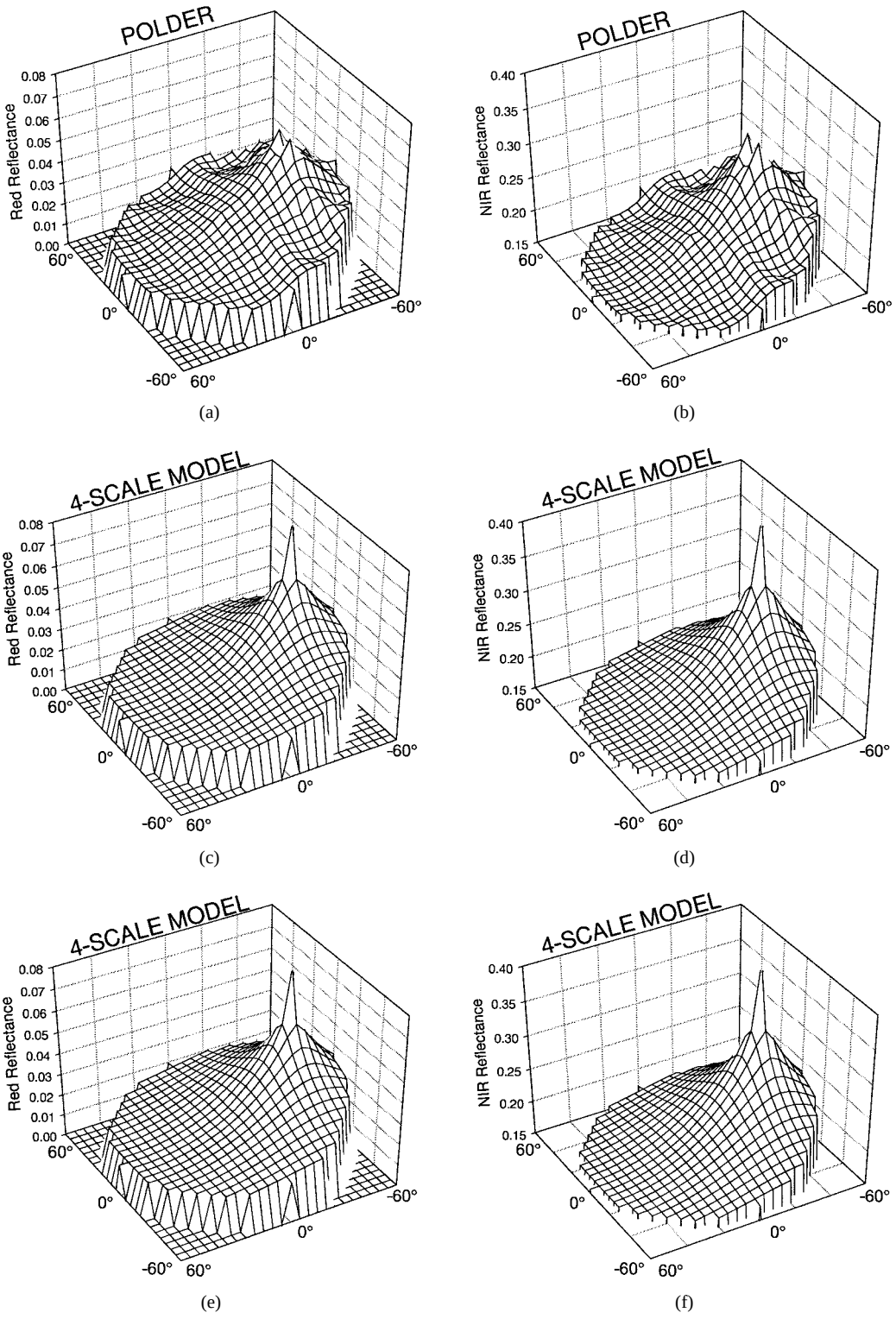

Fig. 9. Old black spruce site: the spatialized POLDER data set in (a) the red and (b) the near-infrared band. The four-scale model (c) red and (d) near-infrared band, and the comparison between the measurements and the model for (e) the red and (f) the near-infrared band.

symmetrical on the two sides of the principal plane. Using this symmetrical assumption, the data were duplicated on the opposite site, giving a mirror effect. Fig. 9(e) and (f) compare the POLDER measurements (x-axis) and the model (y-axis). Each modeled reflectance was done using θ_v, θ_s, and ϕ from the measurements. The diagonal lines represents the one-to-one relationship between the model and the measurements. For the red band, a regression factor R^2 of 0.97 and an rms difference of 0.0022 are computed. As in Fig. 8(a), the lower reflectance values are the ones that are not well simulated, the model overestimating the reflectance on the forwardcattering side. The near-infrared simulation is also very good, with a R^2 of 0.99 and an rms of 0.0058. The lower reflectance values are also overestimated by the model. The regression factors

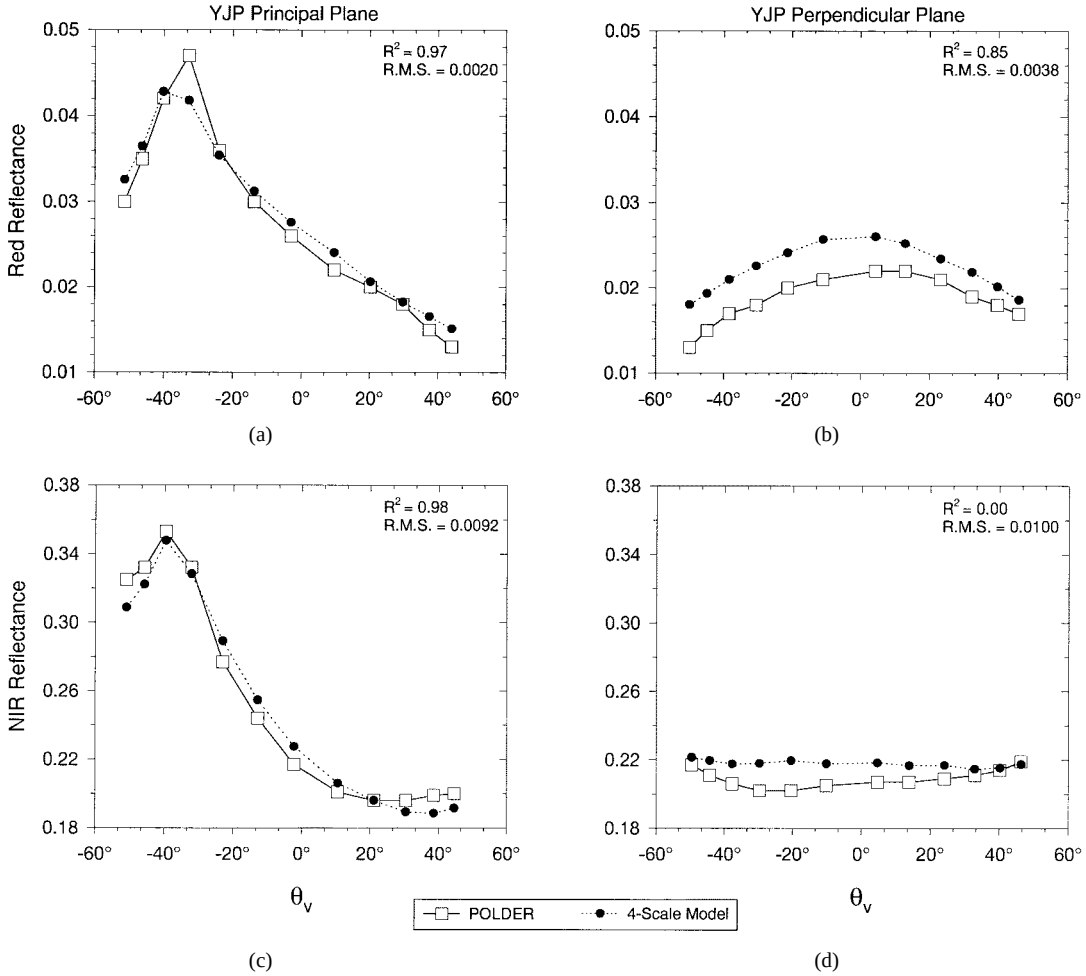

Fig. 10. Comparison between POLDER and the four-scale model for the young jack pine site: (a) principal plane red band, (b) perpendicular plane red band, (c) principal plane near-infrared band, and (d) perpendicular plane near-infrared band.

are close to unity, indicating that the shape of the simulations are in good agreement with the measurements.

2) Young Jack Pine: It was previously found [10] that the Neyman grouping factor (m_2) is about three for an old jack pine forest of 100 × 100 m^2 divided in 100 quadrants. This value of m_2 is used here for both the young and old jack pine sites.

The model mimics the observation closely in both red [Fig. 10(a) and (b)] and near-infrared [Fig. 10(c) and (d)] bands. In Fig. 10(a), the model did not reproduce the measured hotspot, but it must be noted that the largest measured value is usually not exactly at the hotspot because none of the discrete θ_v is equal to θ_s. The red-band principal plane gives a regression factor of $R^2 = 0.97$ with an rms of 0.002. For the perpendicular plane, R^2 is 0.85 and rms is 0.004. The near-infrared simulation is generally in good agreement with R^2 equal to 0.98 and rms of 0.01 for the principal plane. A R^2 value of less than 0.01 was found for the perpendicular plane, and the rms was also 0.01. This means that the curve's shape is not well modeled in the perpendicular plane for the near-infrared band. The two curves diverge on the backscattering side, but the values are very similar. Based on measurements that showed that most shoots were between 10–30° [4], a value of 20° ($\alpha_L = 80°$) for the shoots main axis from the zenith was used in the simulation. The branch inclination was set at 15° from horizontal ($\alpha_b = 15°$). It was observed that the young jack pine simulations were only slightly improved by using the branch architecture; e.g., without the branch architecture [using $G(\theta) = 0.5$ and $\Omega_E = 0.72$], the regression factor was 0.90 for the red-band principal plane.

Fig. 11 has the plots for the spatialized data set compared with the model. The shape of the red reflectance distribution is well modeled, but since the difference, although small (rms is 0.0094), is not systematic, it gives a small regression factor R^2 of only 0.57. The measurements are more scattered than the simulation points. A comparison of the spatialized data near the principal plane in Fig. 11 and the POLDER reflectance measurements in the red band at the BOREAS tower site (Fig. 10) shows that the latter are in the lower values of the spatialized data. The reason may be that the extent of the forest around the site is limited (400–500 m), so some pixels included in the analysis may be of other cover types (mostly clear-cuts with higher red reflectivity). The near-infrared simulations also closely reproduce the measurements with a R^2 of 0.92 and an rms of 0.012. Near-infrared reflectances for the jack pine forest and the surrounding area may be similar.

3) Old Jack Pine: Fig. 12(a) shows that for the red band, in the principal plane, the model results, and the measurements

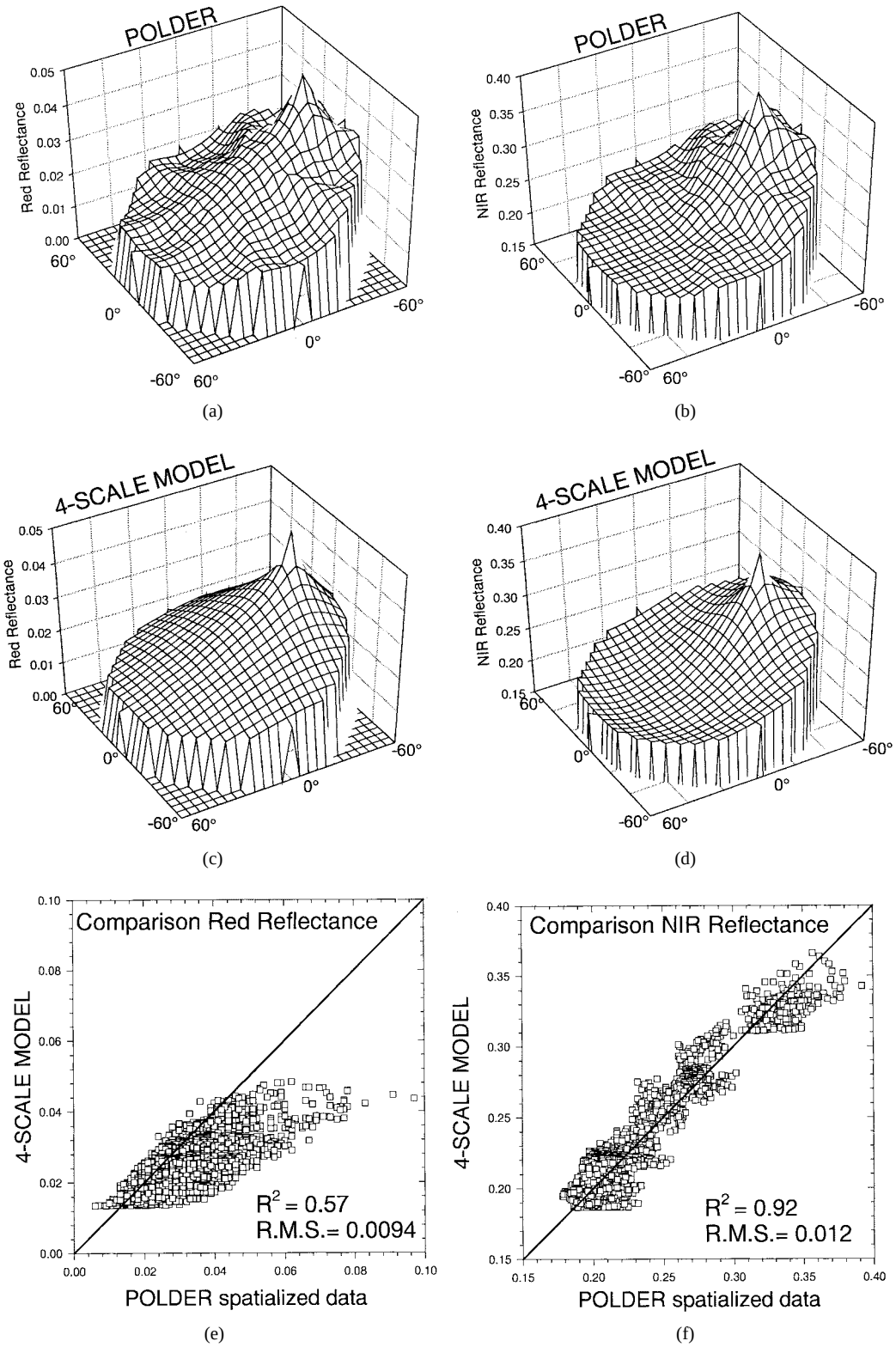

Fig. 11. Young jack pine site: the spatialized POLDER dataset in (a) the red and (b) the near-infrared band. The four-scale model (c) red and (d) near infrared band, and the comparison between the measurements and the model for (e) the red and (f) the near-infrared band.

for the old jack pine site are in excellent agreement (R^2 is larger than 0.99 with an rms of 0.001). The addition of the branch architecture improved the similitude between the model and the measurements for this site. The same branch structure as the young jack pine site was used for the old jack pine trees. In the perpendicular plane [Fig. 12(b)], the two curves have the same inverse bowl shape, but the model overestimates the reflectance, where R^2 is also 0.99 and rms is 0.03. Comparing the measured reflectance in the perpendicular and the principal planes, a sizeable discrepancy is found at nadir. The measured

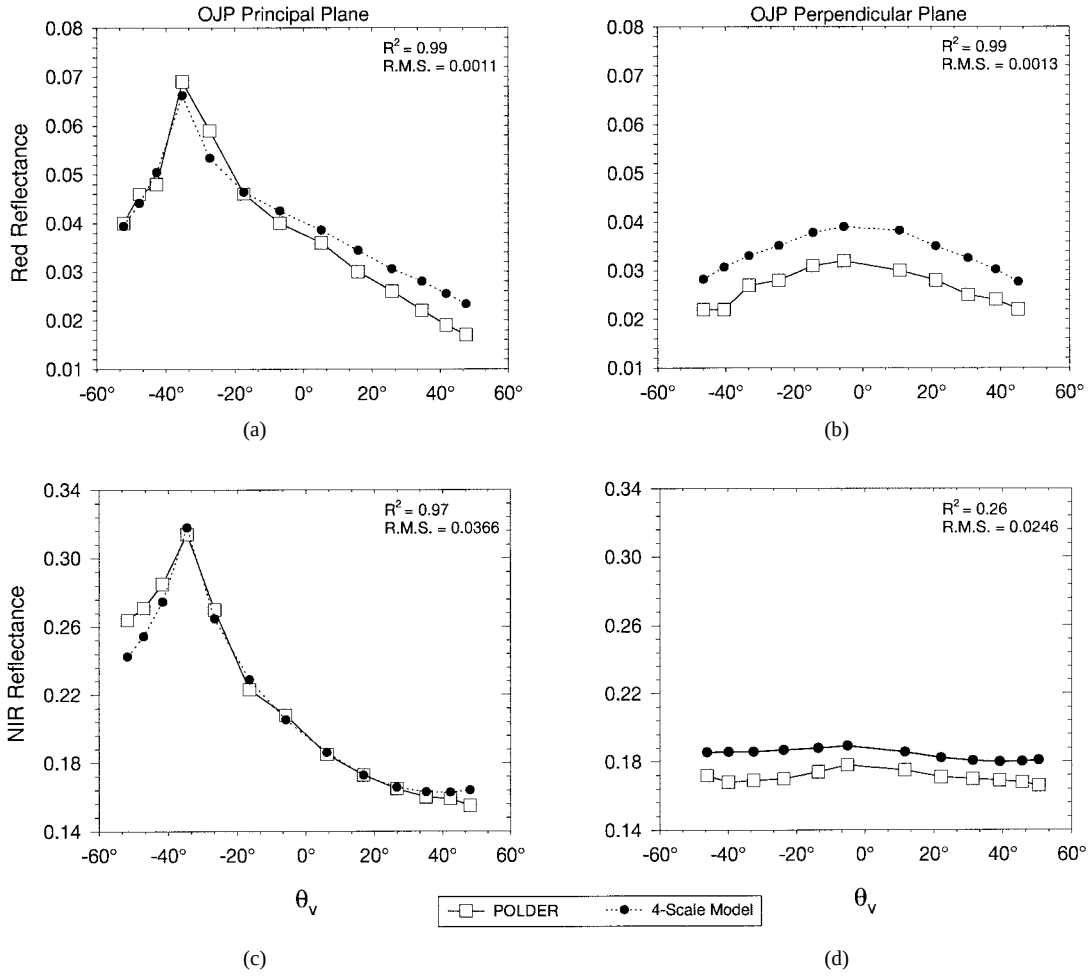

Fig. 12. Comparison between POLDER and four-scale for the old jack pine site: (a) principal plane red band, (b) perpendicular plane red band, (c) principal plane near-infrared band, and (d) perpendicular plane near-infrared band.

reflectance closest to nadir in the principal plane ($\theta_v = 5.1°$ and $\phi = 163.7°$) is 0.036, but the closest data point in the perpendicular plane ($\theta_v = 5.5°$ and $\phi = 208.4°$) is 0.032. The model computes 0.039 for both cases. This difference may be explained by the inhomogeneity of the forest in the vicinity of the tower site. Since a POLDER data point consists of an average of only a few pixels, some difference in the measured reflectance is expected at nadir from different flight lines, which may not exactly overlap at the tower location. In the near-infrared band, the difference between the two planes is smaller at nadir, Fig. 12(c) and (d), than that in the red band, showing good agreements between the measurements and the model for both the principal and perpendicular planes. R^2 is 0.97 for the principal plane, but only 0.26 for the perpendicular plane. The rms is around 0.03 for both simulations.

4) Old Aspen: The old aspen site has a complex structure with distinct overstory and understory. We therefore investigated the contribution of these two layers of foliage to BRDF signature by using single and double versions of the model. In the single-canopy simulations, the reflectivity of the background includes both understory and soil, while in the double-canopy simulations, the understory is treated as a separate layer of vegetation and the background becomes soil only. Physically, the double-canopy is a more accurate representation of this site.

It is shown in Fig. 13(a) and (b) that the BRDF shape of both planes in the reds band BRDF is well reproduced, with R^2 of 0.93 and 0.82 for the double-canopy and 0.94 and 0.82 for the single-canopy. The rms differences between the double-canopy simulation and the data are very good, with 0.0027 for the principal plane and 0.0013 for the perpendicular plane. Slightly larger rms were found for the single-canopy version, with 0.0029 and 0.0039 for the principal and perpendicular planes, respectively.

In the near-infrared band, both versions of the model can reproduce very well most view angles, except for large θ_v values on the backscattering side [Fig. 13(c)]. An underestimation at view angles larger than the sun angle is found. This phenomenon cannot be simulated by the four-scale model without accurate consideration of the multiple scattering effect. The regression factor R^2 are 0.89 and 0.88 for the double and single versions, respectively. The perpendicular simulation gives R^2 of only 0.37 and 0.31, but the rms difference is about the same as for the principal plane, i.e., 0.01 to 0.02.

Overall, both versions performed well and the single-canopy version gives larger reflectance values than the double-canopy

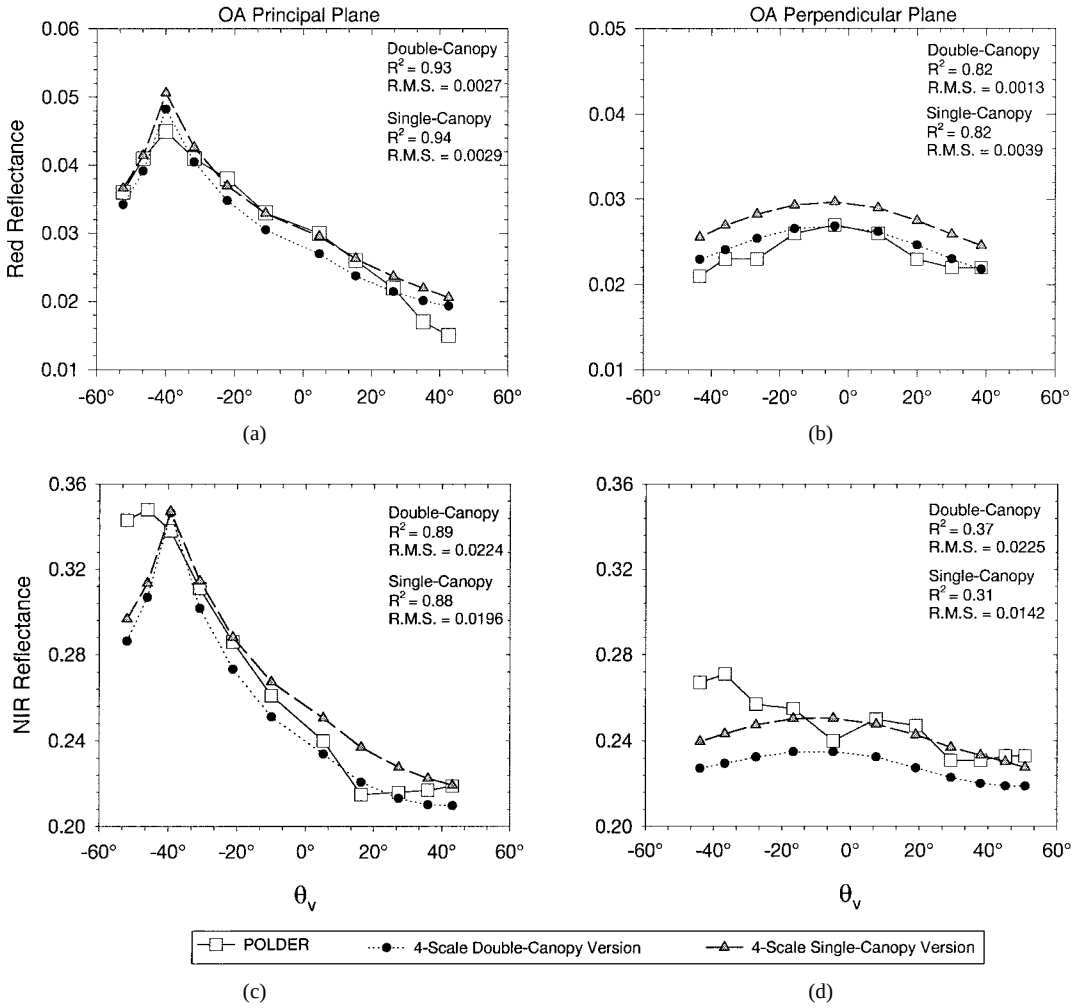

Fig. 13. Comparison between POLDER and simple and doubles canopy version of four-scale for the old aspen site: (a) principal plane red band, (b) perpendicular plane red band, (c) principal plane near-infrared band, and (d) perpendicular plane near-infrared band.

version. This is probably due to the absence of the second canopy; the single-canopy induces less shadow, thus giving a larger reflectance.

IV. Discussion

The model can reproduce BRDF of the different forest canopies remarkably well. The simulations for conifer forests yield better results (R^2 around 0.98 for the principal plane and rms from 0.001 to 0.03) than for the deciduous forest (R^2 around 0.90 for the principal plane and rms from 0.002 to 0.02). This is partly due to the fact that the architectural parameters used were more accurately determined for conifer forests. The black spruce site has more variability in tree height than that in jack pine; this has not been taken into account by the model causing some uncertainties in the simulated results. The spatialized simulations (Figs. 9 and 11) show that the model is able to reproduce the measurements at any view azimuth angles and that the surrounding of the BOREAS young jack pine site is less homogeneous than the site itself, giving a much larger reflectance in the red band.

The young jack pine site was well modeled with or without the branch architecture; the resulting curves were similar in both cases. This is in agreement with the fact that, even with shoots oriented mainly between 10–30° from the zenith, the young jack pine does not exhibit erectophile behavior as much as in the old jack pine [5]. The low foliage density of the old jack pine requires a better representation of the crown architecture to better model the light and view penetration. The larger LAI in the young jack pine prevents the architectural structure from influencing the overall penetration.

A very large W_s was used for the young jack pine site to avoid very sharp hotspots, suggesting that, at this site, subbranch architecture (groups of shoots) may be more important in the estimation of mutual shadows within tree crowns than the individual shoots. Large W_s induces less-clumped canopy based on gap size theories [8], which confirms that the clumping of foliage in branches is less important for that site.

The addition of the branch architecture improved the accuracy of the old jack pine site modeling. Fig. 14 shows how the branch architecture changes the BRDF of the jack pine site in the near-infrared band. The angle distribution of the shoot (20° from the zenith) induces more foliage visible at a large zenith angle, and with a higher reflectivity for the foliage than for the ground, it increases the near-infrared reflectance. The shoot's orientation also decreases the canopy gap fraction near nadir, but at those angles, the canopy view path is done

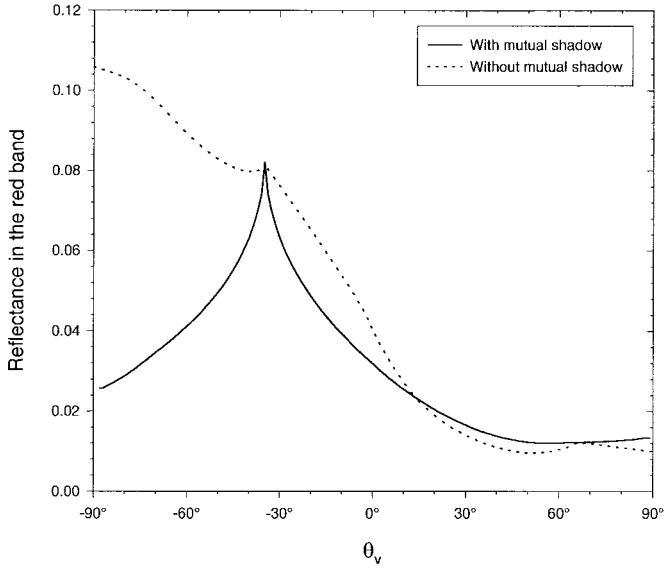

Fig. 14. Simulation of the old black spruce canopy reflectance with and without mutual shadows among shoots on the principal plane, with an angle step of 1° using the parameters of Table I, but with the sun at 35°.

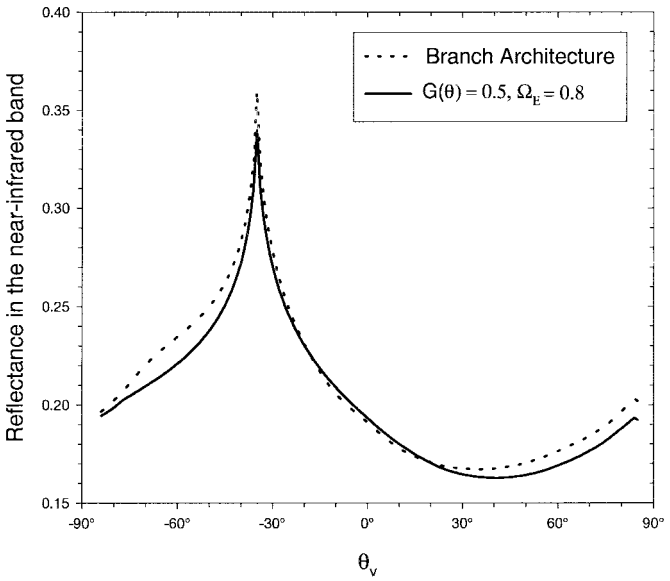

Fig. 15. Branch architecture effect on the principal plane reflectance in the near-infrared band for the old jack pine site.

through multiple layer within the same tree crown. Near nadir, the branch architecture does not change much the proportion of background and canopy viewed (see the gap fraction simulation of Fig. 3). One effect of the branch architecture is to clump the foliage into branches; the difference in the simulated BRDF curves between the case with and without the architecture is small because the branch clumping effect has already been partly considered in the use of Ω_E for the whole stand.

The effect of the Neyman grouping index (m_2) on the reflectance was not investigated much in this paper. Measurements from the old jack pine site revealed a m_2 of three, but the sampling area was too small to really see the grouping effect at large scales. The use of more quadrats can show the importance of the Neyman grouping, but it also has the disadvantage of having smaller quadrats, which can cause computation errors in the gap fraction at large zenith angles when the view line or the solar beam penetration goes beyond the quadrat from the top of the canopy to the ground surface. The Neyman grouping has a strong effect on the gap fraction, but this effect is in part compensated when the total reflectance is computed after the reflectivities are multiplied by the different scene components. Reflectance from forest with a large contract between the background and canopy reflectivity would be more affected by more clumping of trees.

The mutual shadowing of leaves within tree crowns is modeled with $Q_{\rm tot1}$ and $Q_{\rm tot2}$. Although the results are good, it seems that they tend to make the hotspot too sharp, especially at large θ_s (see [10, Figs. 13(c) and 14]). Fig. 15 shows simulations of the principal-plane BRDF of a black spruce forest. Without the mutual shadows between leaves (which is equivalent to having $Q_{\rm tot1} = 1$ and $Q_{\rm tot2} = 0$), we see that the overall shape would be much different. At large view angles, on the backscattering side (negative θ_v), the modeled BRDF does not show a decreasing trend after the hotspot and is too large for θ_v between -40° and 0°. This is often seen at large θ_s because of multiple scattering. In general, red-band BRDF is better simulated than near-infrared-band BRDF, especially near the hotspot. This indicates that the four-scale model can be further improved by considering multiple scattering effects. The model assumes trees of equal height and therefore underestimates the amount of shaded crowns seen. This underestimation could counterbalance the overestimation of shaded foliage computed with $Q_{\rm tot1}$ and $Q_{\rm tot2}$. Four-scale needs to be further developed to consider the enhanced mutual shadows in stands with large tree height variation.

At the old aspen site, the number of hazelnut stems was not an important factor in the resulting BRDF, especially when we put enough hazelnut silhouette to cover the ground (3200 stems/hectare and more). The aspen trees are definitely the dominant factors in the BRDF signature of this site. This explains why the BRDF was also well modeled with the single-canopy version of the model. The probability of seeing the canopy illuminated P_T, or P_{T1} in the case of the double-canopy version, has the general shape of the BRDF curve. The aspen site provides a challenge because of the complexity of the double-canopy feature, but the model is able to simulate it with a reasonable accuracy. Although both the single and double-canopy version of the model gave similar results, the single canopy needed to consider the hazelnut reflectivity as part of the background. The old aspen site also has more multiple scattering than the other sites, and the angular independence of the multiple-scattering effect may cause considerable errors in this case. For such a complex canopy, a more accurate mathematical description of multiple scattering is needed.

V. Conclusion

The four-scale model can be seen as a link between ground and remote-sensing measurements. Although it has many input parameters, it remains relatively simple and a powerful research tool. When some of the parameters are not available

from measurements, the model can be run with fixed general parameters or with best estimates of the missing parameters. More details and better simulations can be achieved when all parameters are available. The measurements taken during BOREAS have helped to show the subtle differences between the four canopies investigated in this paper. Intrinsic structural characteristics of each forest have been incorporated into the model to reproduce the BRDF acquired by POLDER. The branch architecture, as well as a good description of the mutual shadowing of the foliage inside the crown, have shown to be of great importance in the modeling of the BRDF. The branch architecture should be more important for forests with larger contrast between the reflectivities of the background and the canopy than for the jack pine sites that have a bright background. The hotspot signatures were very well modeled, proving that the hotspot kernel based on the canopy gap size distribution is a major improvement over previous hotspot models.

The POLDER instrument has proven to be a very efficient instrument capable of capturing the signatures of different forest canopies. It has the angular and spatial resolutions required to study the hotspot effect. The quality of the measurements is consistent, although some uncertainties still exist in atmospheric correction at large view angles.

With its multiple input parameters, the four-scale model is a flexible tool to study how canopy architecture at each scale influences the reflectance. The reason for the good simulation using only a small parameters set lies in the underlying physics of the interaction between radiation and the canopies described in the model. The parameters and the canopy architecture considerations allow sufficient flexibility of the model to simulate various canopy types. We stress, however, the advantage of this complex model over simpler geometric-optical models in its ability to simulate the BRDF over the entire angle range even with fixed general parameters.

REFERENCES

[1] P. Bicheron, M. Leroy, F. M. Bréon, and O. Hautecoeur, "Enhanced discrimination of boreal forest covers with directional reflectance from the airborne POLDER instrument," *J. Geophys. Res.*, vol. 102, pp. 29 517–29 528, 1997.

[2] F. M. Bréon, V. Vanderbilt, M. Leroy, P. Bicheron, C. L. Walthall, and J. E. Kalshoven, "Evidence of hot-spot signature from airborne POLDER measurements," *IEEE Trans. Geosci. Remote Sensing*, vol. 35, pp. 479–484, Mar. 1997.

[3] E. M. Middleton, S. S. Chan, R. J. Rusin, and S. K. Mitchell, "Optical properties of black spruce and jack pine needles at BOREAS site in Saskatchewan, Canada," *Can. J. Remote Sensing*, vol. 23, no. 2, pp. 188–199, 1996.

[4] J. M. Chen, "Canopy architecture and remote sensing of the fraction of photosynthetically active radiation absorbed by boreal conifer forests," *IEEE Trans. Geosci. Remote Sensing*, vol. 34, pp. 1353–1368, Nov. 1996.

[5] ———, "Optically-based methods for measuring seasonal variation of leaf area index in boreal conifer stands," *Agric. Forest. Meteorol.*, vol. 80, pp. 135–163, 1996.

[6] J. M. Chen and T. A. Black, "Measuring leaf area index of plant canopies with branch architecture," *Agric. Forest. Meteorol.*, vol. 57, pp. 1–12, 1991.

[7] J. M. Chen, P. D. Blanken, T. A. Black, M. Guilbeault, and S. Chen, "Radiation regime and canopy architecture in a boreal aspen forest," *Agri. Forest. Meteorol.*, vol. 86, pp. 107–125, 1996.

[8] J. M. Chen and J. Cihlar, "Quantifying the effect of canopy architecture on optical measurements of leaf area index using two gap size analysis methods," *IEEE Trans. Geosci. Remote Sensing*, vol. 33, pp. 777–787, July 1995.

[9] ———, "Retrieving leaf area index of boreal conifer forest using Lansat TM images," *Remote Sens. Environ.*, vol. 55, pp. 153–162, 1996.

[10] J. M. Chen and S. G. Leblanc, "A four-scale bidirectional reflectance model based on canopy architecture," *IEEE Trans. Geosci. Remote Sensing*, vol. 35, pp. 1316–1337, Nov. 1997.

[11] J. M. Chen, P. M. Rich, S. T. Gower, J. M. Norman, and S. Plummer, "Leaf area index of boreal forests: Theory, techniques, and measurements," *J. Geophys. Res.*, vol. 102, pp. 29 429–29 443, 1997.

[12] J. Cihlar, D. Manak, and N. Voisin, "AVHRR bidirectional reflectance effect and compositing," *Remote Sens. Environ.*, vol. 48, pp. 77–88, 1994.

[13] P.-Y. Dechamps, F. M. Bréon, M. Leroy, A. Podaire, A. Bricaud, J.-C. Buriez, and G. Sève, "The POLDER mission: Instrumental characteristics and scientific objectives," *IEEE Trans. Geosci. Remote Sensing*, vol. 32, pp. 598–613, May 1994.

[14] D. W. Deering, E. M. Middleton, T. F. Eck, and B. P. Banerjee, "Reflectance anisotropy for a spruce-hemlock forest canopy," *Remote Sens. Environ.*, vol. 47, pp. 242–260, 1994.

[15] N. S. Goel and W. Qin, "Influences of canopy architecture on relationships between various vegetation indices and LAI and FPAR: A computer simulation," *Remote Sens. Rev.*, vol. 10, pp. 309–347, 1994.

[16] D. L. B. Jupp and A. H. Strahler, "A hotspot model for leaf canopies," *Remote Sens. Environ.*, vol. 38, pp. 193–210, 1991.

[17] M. Leroy and F. M. Bréon, "Surface reflectance angular signatures from airborne POLDER data," *Remote Sens. Env.*, vol. 57, pp. 97–107, 1996.

[18] X. Li and A. H. Strahler, "Geometric-optical bidirectional reflectance modeling of a coniferous forest canopy," *IEEE Trans. Geosci. Remote Sensing*, vol. GE-24, pp. 906–919, Sept. 1986.

[19] ———, "Modeling the gap probability of a dicontinuous vegetation canopy," *IEEE Trans. Geosci. Remote Sensing*, vol. 26, pp. 161–169, Jan. 1988.

[20] ———, "Geometric-optical bidirectional reflectance modeling of the discrete crown vegetation canopy: Effect of crown shape and mutual shadowing," *IEEE Trans. Geosci. Remote Sensing*, vol. 30, pp. 276–291, Mar. 1992.

[21] X. Li, A. H. Strahler, and C. E. Woodcock, "A hybrid geometric-optical-radiative transfert approach for modeling albedo and directional reflectance of discontinuous canopies," *IEEE Trans. Geosci. Remote Sensing*, vol. 33, pp. 466–480, Mar. 1995.

[22] B. L. Markham, D. L. Williams, J. R. Schafer, F. Wood, and M. S. Kim, "Radiometric characterization of diode-array field spectrometers," *Remote Sens. Environ.*, vol. 51, pp. 317–330, 1995.

[23] E. M. Middleton, D. W. Deering, and S. P. Ahmad, "Surface anisotropy and hemispheric reflectance for a semiarid ecosystem," *Remote Sens. Environ.*, vol. 23, pp. 193–212, 1987.

[24] R. B. Myneni and J. Ross, Eds., *Photon-Vegetation Interactions.* Berlin, Germany: Springer-Verlag, 1991.

[25] J. Neyman, "On a new class of 'contagious' distribution, applicable in entomology and bacteriology," *Ann. Math. Stat.*, vol. 10, pp. 35–57, 1939.

[26] T. Nilson and A. Kuusk, "A reflectance model for the homogeneous plant canopy and its inversion," *Remote Sens. Environ.*, vol. 25, pp. 82–95, 1988.

[27] T. Nilson and U. Peterson, "A forest canopy reflectance model and a test case," *Remote Sens. Environ.*, vol. 37, pp. 131–142, 1991.

[28] J. Otterman and T. W. Brakke, "Dense canopy albedo as a function of illumination direction: Dependance on structure and leaf transmittance," *Theor. Appl. Climatol.*, vol. 43, pp. 3–16, 1991.

[29] C. Barker Schaaf and A. H. Strahler, "Validation of bidirectional and hemispherical reflectance from a geometric-optical model using ASAS imagery and pyranometer measurements of a spruce-forest," *Remote Sens. Environ.*, vol. 49, pp. 138–144, 1994.

[30] P. Sellers, F. Hall, H. Margolis, B. Kelly, D. Baldocchi, D. Den Hartog J. Cihlar, M. Ryan, B. Goodison, P. Crill, J. Ranson, D. Lettermaier, and D. E. Wickland, "The boreal ecosystem-atmosphere study (BOREAS): An overview and early results from the 1994 field year," *Bull. Amer. Meteorol. Soc.*, vol. 76, pp. 1549–1577, 1995.

[31] R. Soffer, "Bidirectional reflectance factors of an open tree canopy by laboratory simulation," M.S. thesis, York Univ., North York, Ont., Canada, 1995.

[32] A. H. Strahler and D. L. B. Jupp, "Modeling bidirectional reflectance of forests and woodlands using Boolean models and geometric optics," *Remote Sens. Environ.*, vol. 34, pp. 153–166, 1990.

[33] W. Verhoef, "Light scattering by leaf layers with application to canopy reflectance modeling: The sail model," *Remote Sens. Environ.*, vol. 16, pp. 125–141, 1984.

[34] E. D. Vermote, D. Tanre, J. L. Deuze, and J. J. Morcrette, "Second simulation of the satellite signal in the solar spectrum: An overview," *IEEE Trans. Geosci. Remote Sensing*, vol. 35, pp. 675–686, Mar. 1997.
[35] H. P. White, J. R. Miller, J. M. Chen, D. R. Peddle, and G. McDermid, "Seasonal change in mean understory reflectance for boreal sites: Preliminary results," in *Proc. 17th Can. Symp. Remote Sensing*, 1995.
[36] A. Wu, Z. Li, and J. Cihlar, "Effect of land cover type and greenness on advanced very high resolution radiometer reflectance: Analysis and removal," *J. Geophys. Res.*, vol. 100, pp. 9179–9192, 1995.

Sylvain G. Leblanc received the B.Sc. degree in physics from the University of Montréal, Montréal, P.Q., Canada, in 1992 and the M.Sc. degree in atmospheric and oceanic sciences from McGill University, Montréal, in 1994, on the remote sensing of turbulence.

He is currently an Environmental Scientist at the Canada Centre for Remote Sensing (CCRS), Ottawa, Ont.. His current research interests include ground truth measurements, remote sensing, modeling and mapping of biophysical properties of forests.

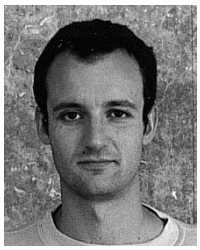

Patrice Bicheron received the Ph.D. degree in 1997 from the Université Paul Sabatier, Toulouse, France.

He worked on the contribution of the multidirectional remote-sensing data for the monitoring of terrestrial vegetation. Its research included the use of this information for the enhancement of the discrimination of boreal forest covers and, more widely, the design and use of physical methods to derive biophysical parameters from natural surfaces. He is currently with the Centre d'Études Spatiales de la BIOsphere (CESBIO), Toulouse, and is in charge of the development of future biophysical products derived from the POLDER instrument.

Jing M. Chen received the B.Sc. degree in 1982 from Nanjing Institute of Meterology, China, and the Ph.D. degree in 1986 from the University of Reading, Reading, U.K.

He is currently a Research Scientist at the Canada Centre for Remote Sensing (CCRS), Ottawa, Ont., Canada, and is an Adjunct Professor at the University of Ottawa and York University, North York, Ont., Canada. His main research interests include turbulence and radiative transfer processes associated with plant canopies. He is currently engaged in research on applications of optical and microwave remote-sensing techniques to boreal ecosystems. The research topics include radiation modeling, biophysical parameters retrieval, and modeling net primary productivity and carbon cycle. He has been a Principal Investigator in Boreal Ecosystem-Atmosphere Study (BOREAS), VEGETATION/SPOT applications and other projects.

Marc Leroy received the Ph.D. degree from Paris VII University, Paris, France, in 1980, in the field of radiatively driven stellar winds.

He became a Research Associate with the Obsevatoire de Paris in 1981 and worked in the field of theoretical plasma physics of the earth's bow shocks, both at the Obsevatoire de Paris and the University of Maryland, College Park. He joined the French Space Agency (Centre National d'Étude Spatiales), Toulouse, France, in 1985 to work on calibration activities associated with the SPOT program, and he became the Head of the Department of Image Quality, Image Processing Division, CNES Technical Centre of Toulouse, in 1989. He joined Laboratoire d'Études et de Recherches en Télédétection Spatiale in 1993, with a specific interest in the physics of remote-sensing measurements in the optical domain, and he is presently in charge of the development of algorithmic chains of land surface products of the POLDER instrument at the Centre d'Études Spatiales de La Biosphère (CESBIO), Toulouse.

Josef Cihlar (M'86–SM'88) received the B.Sc. Agr. degree in agricultural engineering, the M.Sc. degree in soil science, and the Ph.D. degree in geography and remote sensing.

Between 1975 and 1991, he worked as a Scientist and head of the Applications Development Section at the Canada Centre for Remote Sensing, Ottawa, Ont.. Presently, he is a Research Scientist and head of CCRS Environmental Monitoring Section. His research interests focus on the use of satellite observations for monitoring and modeling environmental change over land at regional to continental scales. He has been involved in several interdisciplinary projects including Boreal Ecosystem-Atmosphere Study (BOREAS) and the Northern Biosphere Observation Modeling Experiment (NBIOME).